Photon-Impenetrable, Electron-Permeable: The Carbon Nanotube Forest as a Medium for Multiphoton Thermal-Photoemission

Mehran Vahdani Moghaddam,[†] Parham Yaghoobi,[†] George A. Sawatzky,[‡] and Alireza Nojeh*[,†]

[†]Department of Electrical and Computer Engineering; [‡]Department of Physics and Astronomy, and Department of Chemistry, University of British Columbia, Vancouver, BC V6T 1Z4, Canada

ABSTRACT Combining the photoelectric and thermionic mechanisms to generate free electrons has been of great interest since the early days of quantum physics as exemplified by the Fowler–DuBridge theory, and recently proposed for highly efficient solar conversion. We present experimental evidence of this combined effect over the entire range spanning room-temperature photoemission to thermionic emission. Remarkably, the optical stimulus alone is responsible for both heating and photoemission at the same time. Moreover, the current depends on optical intensity quadratically, indicating two-photon photoemission, for intensities of *ca.* 1–50 W/cm^2, which are orders of magnitude below the intensities required for two-photon photoemission from bulk metals. This surprising behavior appears to be enabled by the internal nanostructure of the carbon nanotube forest, which captures photons effectively, yet allows electrons to escape easily.

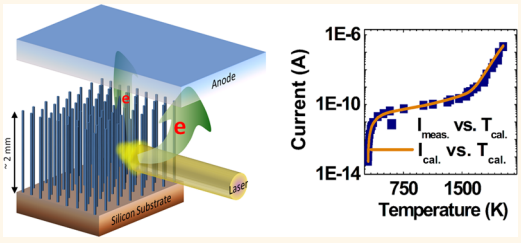

KEYWORDS: generalized Fowler–DuBridge theory · carbon nanotube forest · thermionic emission · two-photon photoemission · electron escape depth · solar cell

Photoexcitation and thermal excitation of electrons (photoemission and thermionic emission) are of fundamental interest and ubiquitous in applications—from optoelectronics, photonics, and vacuum electronics to thermionics, thermoelectrics, and photovoltaics. The combination of light and heat in creating free electrons has also been studied since the first half of the previous century, notably with the works of Fowler and DuBridge,[1−3] and this interest has continued over the decades through, for instance, the generalization of the Fowler–DuBridge model of photo/thermal emission[4] and the development of models for the combined effects of light, heat, and field on emission.[5] Recently, this combination has gained broader appeal due to the opportunities it offers for applications such as the efficient conversion of light to electricity:[6] if the optically generated heat in a solar cell could be used to promote electronic excitations, efficiency could be improved significantly. Notably, photon-enhanced thermionic emission (PETE) of electrons into vacuum has recently been proposed as a mechanism for efficient solar energy conversion[7,8] and the behavior of the photoemission current predicted over a wide range of temperatures (Figure 1).

However, this behavior, spanning room-temperature photoemission all the way to thermionic emission, has not yet been reported experimentally. For a material to exhibit this combined photo/thermal excitation of electrons in a noticeable manner, it should (1) be able to withstand very high temperatures, (2) be an excellent photon absorber, (3) have reasonable photoelectric quantum efficiency, and (4) allow the electrons to escape effectively from any depth where photons are absorbed. The combination of these requirements is not found easily in bulk materials. For example, in metal photocathodes, due to electron–electron interactions, the electron escape depth is very low and a significant portion of the excited electrons are unable to escape. In addition, ideally the candidate material would use the light-induced heat itself to

* Address correspondence to anojeh@ece.ubc.ca.

Received for review January 7, 2015 and accepted March 3, 2015.

Published online March 13, 2015
10.1021/acsnano.5b00115

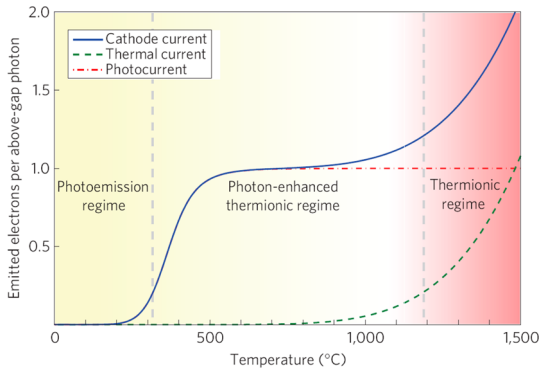

Figure 1. Photoemission current as a function of cathode temperature, showing the photon-enhanced thermionic emission (PETE) effect. Reprinted with permission from ref 7. Copyright 2010 Nature.

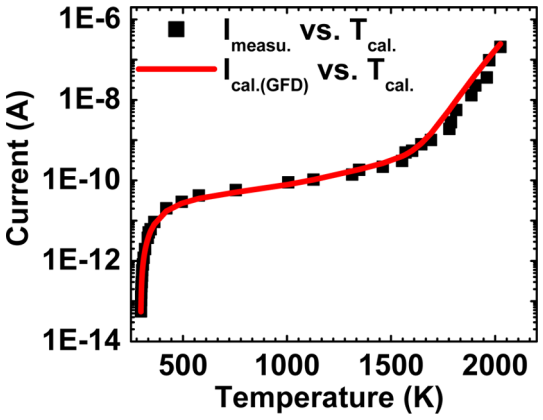

Figure 2. Measured electron emission current as a function of the temperature of the illuminated spot. Note the similarity with the PETE[7] current as predicted in Figure 1. The solid line shows the current calculated using the Generalized Fowler–DuBridge model,[4] which shows a good match to the measured values.

enhance photoelectron emission, rather than lose it to thermal conduction. In the present paper, we show that carbon nanotube forests appear to satisfy the above criteria and are thus an excellent candidate for the manifestation of this emission behavior.

Good levels of photoemission and thermionic emission from carbon nanotubes have previously been reported.[9−14] It has also been shown that carbon nanotube forests are among the best photon absorbers (darkest materials) over a broad spectral range.[15,16] Our previous simulations using the effective optical properties of nanotube forests[17] have revealed that, for light polarized parallel to the nanotubes' axis, the absorption length is only on the order of a few tens of nanometers.[18] We have also observed a unique, localized light-induced heating in nanotube forests (the "Heat Trap" effect)[19] that locks in optically generated heat and allows the attainment of very high temperatures using modest optical intensities of only a few tens of W/cm^2 (and photon energies well below the workfunction), that is 3−4 orders of magnitude lower than what is required for significant optical heating in bulk conductors. This effect is counterintuitive, as nanotubes are understood to have high thermal conductivity. We have explained this peculiar behavior based on the quasi-one-dimensional nature of heat transfer in the nanotube forest and a strongly temperature-dependent thermal conductivity (decreasing with temperature at high temperatures).[20] Thus, as the optical intensity reaches a certain threshold (which is still orders of magnitude lower than that required for significant heating of a bulk conductor), a positive feedback mechanism drives down the local thermal conductivity and raises the temperature of the illuminated spot rapidly. We have previously presented a model that explains the experimental outcomes of the "Heat Trap" effect well based on this mechanism.[20]

Here, we present results using a 266 nm continuous-wave (CW) laser in a broad intensity range of ∼0.1−110 W/cm^2. The associated photon energy (4.66 eV) is sufficient to induce photoemission from carbon nanotubes, and the "Heat Trap" effect also naturally takes place, serving as a mechanism to heat the nanotubes, thus enabling the study of the combined effects of heat and light on the electron emission behavior. The nanotube forest in use is a macroscopic object, with lateral dimensions of ∼5 mm and a height of ∼2 mm, and only a small spot on the sidewall of the forest is illuminated. The Methods section describes the experimental details.

RESULTS AND DISCUSSION

Figure 2 shows our measured photoemission current as a function of temperature, experimentally confirming a behavior similar to the PETE curve (compare with Figure 1). The solid line on the graph shows the excellent fit of the data to the generalized Fowler−DuBridge (GFD) theory of photo/thermal emission[4] over the entire range of optical intensities (and resulting temperatures) studied. This is the first experimental confirmation of this theory over this wide temperature range, spanning all possible regimes. We also show the surprising result that a significant portion of the emission current appears to be the result of two-photon photoemission (2PPE), which has not been observed in any other material at the low optical intensities used here, which are ∼10 W/cm^2 and from a CW, rather than pulsed, laser. (Typically, pulsed lasers with pulse intensities on the order of MW/cm^2 are used in order to induce multiphoton photoemission.[21−24] Thus, we observe one-photon photoemission (1PPE) at low intensities, thermionic emission at high intensities, and an intermediate regime dominated by 2PPE. As we shall see, the key underlying enabler appears to be the internal, mostly empty, nanostructure of the forest.

Figure 3a shows the emission current *versus* laser intensity on a log−log scale. At low intensities, a slope of 1 is observed. At intermediate intensities, the slope is

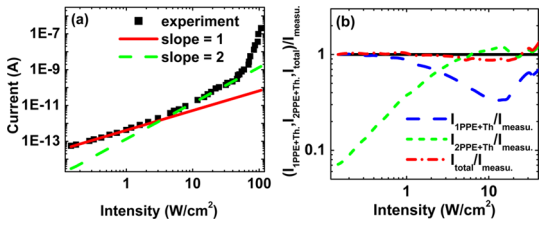

Figure 3. (a) Electron emission current as a function of laser intensity. (b) The ratio of best GFD fits to experimental data assuming the electron emission to be due to only 1PPE and thermionic (long-dash blue curve), 2PPE and thermionic (short-dash green curve), and all three processes, 1PPE, 2PPE and thermionic (= I_{total}, short-dash-dot red curve). Clearly, all three mechanisms are needed in order to fit the entire range of intensities.

2 (suggesting 2PPE) and, at high intensities, thermionic emission becomes dominant.

According to the GFD model, the current density of an emitter can be written as a sum of partial currents[4] as

$$J = \sum_{n=0}^{\infty} a_n \left(\frac{e}{hv}\right)^n A_G I^n (1 - R_v)^n T^2 F\left(\frac{nhv - \varphi}{kT}\right) \quad (1)$$

where e is the electron charge, n is the order of the photoemission process, a_n depends on the sample and reflects the probability of n-photon photoemission, A_G is Richardson's constant, hv is the photon energy, φ is the workfunction, R_v is the material's reflectivity at frequency v, k is Boltzmann's constant, T is the absolute temperature of the emission area (obtained as described in the Methods section), I is the incident laser intensity, and $F(x)$ is the Fowler function.[1] The partial currents corresponding to n = 0, 1, and 2 are due to thermionic, 1PPE, and 2PPE processes, respectively.

We note that a more general formulation exists that combines the effects of heat, field, and photons on electron emission.[5] However, in our experiments there is no field-emission, photofield-emission or optical field-emission effect: the applied collection voltage to the anode is 10 V, and the anode is separated from the nanotube forest by 3 mm, translating to an applied field of 3.3×10^3 V/m, which is 3 orders of magnitude lower than the typical value of $\sim 10^6$ V/m (taking into account the field enhancement by nanotubes) required for any field-emission related effect in nanotubes. Similarly, the maximum laser intensity used in our measurements is 110 W/cm^2, which translates to a maximum electric field amplitude of 2.9×10^4 V/m, again 2 orders of magnitude lower than the levels needed for any significant optical/photofield-related effect. Moreover, the electric field of the laser does not act for a long enough time in any given direction to free the electrons from the nanotubes; the Keldysh parameter can be estimated to be $\sim 2.8 \times 10^8$, confirming the lack of field-related effects. The other point to note is that the GFD model was developed for bulk emitters. Its application to quasi-one-dimensional materials such as nanotubes thus requires caution. However, in the case of the nanotube forest, one expects the collective behavior of millions of nanotubes (which are interacting in the forest and are all illuminated simultaneously) to determine the emission behavior; the forest effectively constitutes a "bulk" structure. This motivates the use of the GFD model in this case.

As can be seen from Figure 3b, it is not possible to fit the entire range of data using only n = 0 and 1 terms (long-dash blue curve): expecting the electron emission process to be 1PPE at low temperatures and thermionic at high temperatures, any attempt to find values for a_1 and φ that can fit these regions will lead to significant deviation from the data points at intermediate intensities. Similarly, using only n = 0 and 2 terms misses out on the low-intensity part of the curve (short-dash green curve). A satisfactory fit to the entire range of data is possible only by including both 1PPE and 2PPE processes in addition to the thermionic process (short-dash-dot red curve). It can also be seen that 1PPE is dominant at low intensities and 2PPE at intermediate intensities; at high intensities their contributions are comparable.

The values of the parameters used to obtain the best fit in Figure 3 are $a_1 = 3.8 \times 10^{-20}$ (m^{2}s/C), $a_2 = 6.20 \times 10^{-28}$ (m^{2}s/C)^2, and $\varphi = 4.62$ eV. Remarkably, this value of a_2 is several orders of magnitude larger than those reported for bulk metals such as Ta, Mo, and W,[4] allowing nanotubes to exhibit 2PPE at such low optical powers. We now attempt to provide an explanation for this high value of the 2PPE coefficient in nanotube forests.

Consider the fact that, in the nanotube forest, the average distance between the nanotubes is 3−4 times the average nanotube diameter[25] and, thus, over 90% of the forest consists of empty space (Figure 4a) (see the Methods section for a more detailed description of the forest structure). Similar levels of sparsity for nanotube forest have also been reported in the literature.[26,27] This leads to a substantially higher electron escape depth in the forest than in regular metals. (We have previously observed unusually high electron penetration depths of tens of micrometers in nanotube forests in the context of secondary and backscattered electron generation and transport.[25] Although those studies were concerned with the much higher electron kinetic energies relevant to electron microscopy, they still demonstrate the essential point that the hollow structure of the nanotube forest allows electrons to travel unusually long distances compared to what we see in bulk metals.) Thus, the electrons excited in regions deep within the forest may have a chance to travel to the top surface of the forest and be collected directly by the anode overhead. The arrow emanating from the top of the forest and going toward the anode on Figure 4b represents the paths of such electrons.

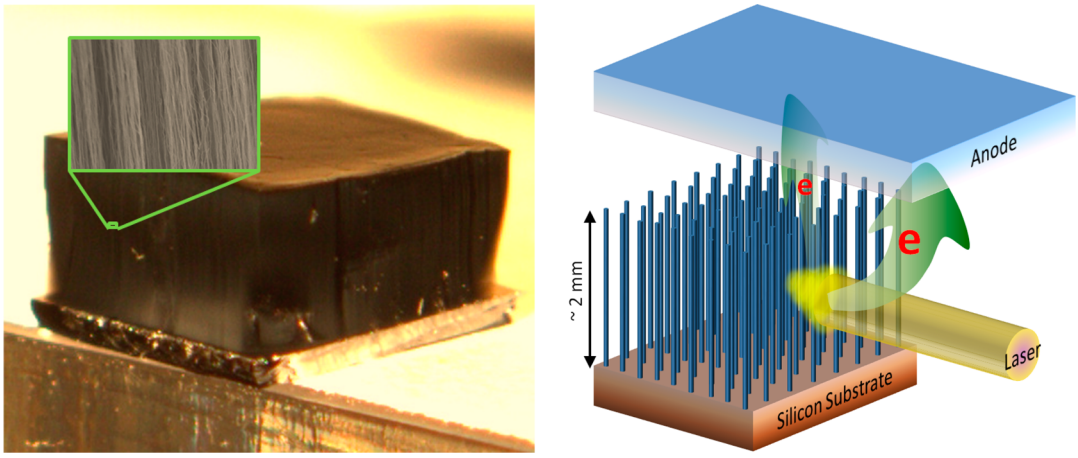

Figure 4. (Left) A photo of a carbon nanotube forest over 2 mm tall and 5 mm on each side (note the silicon substrate with a thickness of 0.5 mm), effectively forming a macroscopic object. Inset is a scanning electron micrograph of the sidewall of the forest, showing the overall alignment of the nanotubes and the significant internanotube distance. (Right) A schematic of the experiment, showing the electrons exiting from the sidewall of the forest, as well as those emerging from the top surface of the forest.

Another effect concerns the electrons emitted out of the sidewall surface of the forest, directly from the point of laser incidence (represented by the arrow starting from the sidewall of the forest and curving upward toward the anode on Figure 4b). For these, we offer the following explanation: consider Spicer's three-step volume photoemission model.[28] These steps consist of optical absorption, electron transport, and electron escape. Accordingly, the 2PPE yield is proportional to

$$a_2 = \eta \frac{\frac{\alpha_{2PPE}}{\alpha} P_{Esc}}{\left(2 + \frac{l}{L}\right)} \qquad (2)$$

Here, α_{2PPE} represents the two-photon absorption coefficient, α is the total optical absorption coefficient of the solid and determines the absorption length ($l = 1/\alpha$), P_{Esc} is the electron escape probability, L is the electron escape length and is characterized by inelastic scattering of photoexcited electrons (*e.g.*, electron−electron and electron−phonon scattering), and η is related to atomic and optical constants. All parameters are functions of the photon energy. To have a high 2PPE yield, one needs a large α_{2PPE}/α, a large P_{Esc}, and a small l/L. α_{2PPE}/α is the ratio of two-photon absorption events resulting in an electron gaining enough energy to go above the vacuum level, to all optical absorption events. We do not have a reason to believe that this ratio should be particularly high in nanotubes (although we do not exclude such a possibility). Instead, the dominant effect here may come from l/L. If the electron escape depth is comparable to or larger than the optical absorption depth, a significant fraction of the excited electrons will be able to escape. However, in metals electron−electron interactions reduce the escape depth: due to the availability of a continuum of empty states, the photoexcited electrons can easily lose energy to valence electrons. Most of these valence electrons will be excited to levels below the vacuum level and cannot escape (the excess energy of the initial electron will not be sufficient to excite a valence electron to above the vacuum level and itself also stay above the vacuum level). As a result, the electron escape depth could be extremely small. For example, in Cs, when excited with a photon energy of 1 eV greater than the workfunction, the electron escape depth is about 10 A. In the nanotube forest, on the other hand, as discussed before, the electron escape depth could be high due to the empty space within the forest. Nanotube forests are also excellent optical absorbers, and we have previously predicted that light polarized parallel to the nantoubes' axis is absorbed within only a few tens of nanometers.[18] Therefore, l/L may be relatively small in the nanotube forests.

Another way to understand this is that the photon wavelength in use (266 nm) is about an order of magnitude larger than the internanotube spacing (a few tens of nanometers), while the typical wavelength of the 2PPE electrons, which have kinetic energies of a few eV, is on the order of a few nanometers and thus about an order of magnitude smaller than the internanotube spacing in the forest. Therefore, the photons essentially see the environment as impenetrable and are almost entirely captured by the first few layers of nanotubes that they encounter, whereas the 2PPE electrons can permeate through the empty spaces in between the nanotubes and escape effectively. The situation is not as favorable for 1PPE electrons, which have smaller kinetic energies and thus larger wavelengths. We believe this is the reason why the a_1 coefficient is not unusually large.

It is also possible to have a contribution from P_{Esc}. For a bulk metal, electron escape to the outside happens after the electron has potentially lost significant energy

inside the material. In the nanotube forest, on the other hand, the actual emission to vacuum could happen very close to the excitation point (on the surface of each nanotube). Therefore, a larger P_{Esc} may be expected for the nanotube forest.

We also performed a stopping voltage (negative anode voltage that blocks all emitted electrons) test. In the linear part of the current−intensity curve, we obtained 0.45 V independently of the laser intensity, consistent with 1PPE. At higher intensities, the stopping voltage gradually increased with intensity—not surprising given the corresponding increase in the temperature—reaching 1.29 V at 50 W/cm^2. Given that the energy of the illuminating photons is very close to the estimated nanotube workfunction, the electrons emitted due to 1PPE must either originate from the Fermi tail or have suffered little energy loss inside the nanotubes prior to emission (surface photoemission). 2PPE, on the other hand, could be contributed to by a large volume of the forest, as a result of which the electrons escaping from deeper regions could lose some energy before leaving the forest. This might explain why the difference of the two stopping voltages is less than one photon energy. Another factor is that electrons leaving the nanotube forest surface toward the anode do not necessarily exit perpendicularly to the surface, but part of their kinetic energy could be in the lateral directions.

Finally, we briefly return to Figure 2, which also shows a plot of the emission current as a function of the emission spot temperature, obtained using eq 1. Note that the calculation of the spot temperature does not involve the use of the GFD model (see the Methods section). Therefore, this figure shows the quality of the GFD fit as a function of temperature over this wide range of temperatures.

CONCLUSION

We studied electron emission from carbon nanotube arrays illuminated with a continuous-wave, ultraviolet laser. In sharp contrast to the situation in bulk cathodes where one only observes linear photoemission in the range of intensities used here, we observed three regions corresponding to 1PPE, 2PPE, and thermionic emission, all happening only due to this single light source. We also observed that the emission current closely follows the GFD law of temperature-dependent multiphoton photoemission over the entire range of intensities (and resulting temperatures) studied. We believe the unique behavior observed is largely because of the internal nanostructure of the forest, which consists of mostly empty space in between the nanotubes. The resulting material property that photons are captured and electrons escape effectively is of fundamental importance for the conversion of light to electricity in applications ranging from photocathodes to solar cells. The insight gained from these results opens a new door for engineering other nanostructured materials with similar properties for various applications.

METHODS

We used atmospheric pressure chemical vapor deposition (CVD) to grow multiwall carbon nanotube forests with lateral dimensions of ∼5 mm and heights of ∼2 mm on a silicon substrate (Figure 4a). A highly p-doped silicon wafer was used as substrate, on which a growth catalyst was first deposited. The catalyst layer consisted of a layer of iron approximately 2 nm in thickness over approximately 10 nm of alumina, both deposited using electron beam evaporation. The ethylene-based CVD apparatus comprised a furnace zone to preheat the gases to 850 °C, and a resistive substrate heater to heat the substrate (which included the catalyst layer) to 800 °C. A typical process involved 1 min of annealing under 800 sccm of argon and 800 sccm of hydrogen, and then the growth phase using 400 sccm of ethylene for a duration of approximately 20 min. As a result, vertically aligned nanotube forests with heights of ∼2−3 mm were obtained. Electron microscopy revealed the nanotubes to be multiwall with diameters in the 10 nm order of magnitude and internanotube spacing several times larger than nanotube diameter, typically in the 50 nm order of magnitude. Given that the nanotubes are arranged in a two-dimensional array, this means that the fill ratio of nanotubes in the forest is $(10/50)^2 = 0.04 = 4\%$, and that over 90% of the volume of the forest is empty space, with the mass density of the forest being on the order of 0.02−0.04 g/cm^3. We have also concluded this from liquid-induced shrinkage experiments: upon introducing a liquid to the nanotube forest and letting it dry, the nanotubes are drawn together due to the capillary action, and the forest thus shrinks to a structure where the nanotubes are closely packed. It is seen that the lateral dimensions of the forest shrink by a factor of 4−5 in this manner, confirming that before shrinkage the forest included more than 90% empty space. A Spectra-Physics Wavetrain frequency doubler generated a CW 266 nm (UV) beam from the 532 nm (green) output of a Coherent Verdi V5 CW laser. A fused-silica lens was used to focus the beam (with electric field polarized parallel to the nanotubes' axis) onto a spot on the side surface of the nanotube forest, which was situated inside a high-vacuum chamber (pressure ≈ 10^{-8} Torr), *via* a sapphire viewport with a transparency of ∼72% at 266 nm. The beam (normal incidence) spot was circular, with a radius of ∼70 μm at the point of incidence. The nanotube forest served as cathode, while a copper counter electrode, mounted above the top surface of the nanotube forest at a distance of ∼3 mm, served as anode. A Keithley 6430 subfemtoamp remote sourcemeter was used to apply 10 V of collection voltage to the anode and measure the emission current through the cathode. The vacuum chamber was placed inside a Faraday shield to reduce noise and enable a current measurement sensitivity of 3 fA.

To estimate the coefficients a_n in eq 1, knowledge of the temperature of the illuminated spot is required. We recorded the spectrum of its incandescent glow using an Ando AQ-6315A optical spectrum analyzer and fit it to Planck's blackbody radiation formula. Owing to the wavelength range limitation of the spectrometer, we could only measure temperatures higher than ∼1280 K. To obtain the temperature in the entire range needed (down to room temperature), we employed a model described previously[19,20] and the measured temperatures to deduce the parameters of the model, and subsequently calculated the temperature for the entire range of optical intensities used (Figure 3).

Conflict of Interest: The authors declare no competing financial interest.

Acknowledgment. We acknowledge financial support from the Natural Sciences and Engineering Research Council, the Canada Foundation for Innovation, the British Columbia Knowledge Development Fund, the BCFRST Foundation, and the British Columbia Innovation Council. Parham Yaghoobi thanks the Department of Electrical and Computer Engineering and the University of British Columbia for additional support. Alireza Nojeh is grateful to the Peter Wall Institute for Advanced Studies for additional support. We also thank L. Chrostowski and N.A.F. Jaeger for making their optical spectrum analyzer available to us.

REFERENCES AND NOTES

1. Fowler, R. H. The Analysis of Photoelectric Sensitivity Curves for Clean Metals at Various Temperatures. *Phys. Rev.* **1931**, *38*, 45–56.
2. DuBridge, B. L. A. A Further Experimental Test of Fowler's Theory of Photoelectric Emission. *Phys. Rev.* **1932**, *39*, 108–118.
3. DuBridge, B. L. A.; Roehr, W. W. Photoelectric and Thermionic Properties of Palladium. *Phys. Rev.* **1932**, *39*, 99–107.
4. Bechtel, J. H.; Smith, W. L.; Bloembergen, N. Two-Photon Photoemission from Metals Induced by Picosecond Laser Pulses. *Phys. Rev. B* **1977**, *15*, 4557–4563.
5. Jensen, K. L. General Formulation of Thermal, Field, and Photoinduced Electron Emission. *J. Appl. Phys.* **2007**, *102*, 024911–024921.
6. Smestad, G. P. Conversion of Heat and Light Simultaneously Using a Vacuum Photodiode and the Thermionic and Photoelectric Effects. *Sol. Energy Mater. Sol. Cells* **2004**, *82*, 227–240.
7. Schwede, J. W.; Bargatin, I.; Riley, D. C.; Hardin, B. E.; Rosenthal, S. J.; Sun, Y.; Schmitt, F.; Pianetta, P.; Howe, R. T.; Shen, Z.-X.; *et al*. Photon-Enhanced Thermionic Emission for Solar Concentrator Systems. *Nat. Mater.* **2010**, *9*, 762–767.
8. Schwede, J. W.; Sarmiento, T.; Narasimhan, V. K.; Rosenthal, S. J.; Riley, D. C.; Schmitt, F.; Bargatin, I.; Ahasrabuddhe, K.; Howe, R. T.; Harris, J. S.; et al. Photon-Enhanced Thermionic Emission from Heterostructures with Low Interface Recombination. *Nat. Commun.* **2013**, *4*, 1576–1581.
9. Wong, T.-H.; Gupta, M. C.; Hernandez-Garcia, C. Nanosecond Laser Pulse-Induced Electron Emission from Multiwall Carbon Nanotube Film. *Nanotechnology* **2007**, *18*, 135705–135707.
10. Westover, T. L.; Franklin, A. D.; Cola, B. A.; Fisher, T. S.; Reifenberger, R. G. Photo- and Thermionic Emission from Potassium-Intercalated Carbon Nanotube Arrays. *J. Vacuum Sci. Technol. B* **2010**, *28*, 423–434.
11. Purcell, S. T.; Vincent, P.; Journet, C.; Binh, V. T. Hot Nanotubes: Stable Heating of Individual Multiwall Carbon Nanotubes to 2000 K Induced by the Field-Emission Current. *Phys. Rev. Lett.* **2002**, *88*, 105502–105505.
12. Cox, D. C.; Forrest, R. D.; Smith, P. R.; Silva, S. R. P. Thermionic Emission from Defective Carbon Nanotubes. *Appl. Phys. Lett.* **2004**, *85*, 2065–2067.
13. Wei, Y.; Jiang, K.; Feng, X.; Liu, P.; Liu, L.; Fan, S. Comparative Studies of Multiwalled Carbon Nanotube Sheets before and after Shrinking. *Phys. Rev. B* **2007**, *76*, 045423–045429.
14. Yaghoobi, P.; Michan, M.; Nojeh, A. Middle-Ultraviolet Laser Photoelectron Emission from Vertically Aligned Millimeter-Long Multiwalled Carbon Nanotubes. *Appl. Phys. Lett.* **2010**, *97*, 153119–153121.
15. Yang, Z.-P.; Ci, L.; Bur, J. A.; Lin, S.-Y.; Ajayan, P. M. Experimental Observation of an Extremely Dark Material Made by a Low-Density Nanotube Array. *Nano Lett.* **2008**, *8*, 446–451.
16. Mizuno, K.; Ishii, J.; Kishida, H.; Hayamizu, Y.; Yasuda, S.; Futaba, D. N.; Yumura, M.; Hataa, K. A Black Body Absorber from Vertically Aligned Single-Walled Carbon Nanotubes. *Proc. Natl. Acad. Sci. U.S.A.* **2009**, *106*, 6044–6047.
17. Vidal, F. J. G.; Pitarke, J. M.; Pendry, J. B. Effective Medium Theory of the Optical Properties of Aligned Carbon Nanotubes. *Phys. Rev. Lett.* **1997**, *78*, 4289–4292.
18. Vahdani Moghaddam, M.; Yaghoobi, P.; Nojeh, A. Polarization-Dependent Light-Induced Thermionic Electron Emission from Carbon Nanotube Arrays Using a Wide Range of Wavelengths. *Appl. Phys. Lett.* **2012**, *101*, 253110–253114.
19. Yaghoobi, P.; Vahdani Moghaddam, M.; Nojeh, A. Heat Trap: Light-Induced Localized Heating and Thermionic Electron Emission from Carbon Nanotube Arrays. *Solid State Commun.* **2011**, *151*, 1105–1108.
20. Yaghoobi, P.; Vahdani Moghaddam, M.; Nojeh, A. Solar Electron Source and Thermionic Solar Cell. *Am. Inst. Phys. Adv.* **2012**, *2*, 042139–042150.
21. Bechtel, J. H.; Smith, W. L.; Bloembergen, N. Four-Photon Photoemission from Tungsten. *Opt. Commun.* **1975**, *13*, 56–59.
22. Musumeci, P.; Cultrera, L.; Ferrario, M.; Filippetto, D.; Gatti, G.; Gutierrez, M. S.; Moody, J. T.; Moore, N.; Rosenzweig, J. B.; Scoby, C. M.; *et al*. Multiphoton Photoemission from a Copper Cathode Illuminated by Ultrashort Laser Pulses in an RF Photoinjector. *Phys. Rev. Lett.* **2010**, *104*, 084801–084804.
23. Logothetis, M.; Hartman, P. L. Laser-Induced Electron Emission from Solids: Many-Photon Photoelectric Effects and Thermionic Emission. *Phys. Rev.* **1969**, *187*, 460–474.
24. Ferrini, G.; Viggiani, A.; Sertore, D.; Michelato, P.; Parmigiani, F. Linear and Nonlinear Total-Yield Photoemission Observed in the Subpicosecond Regime in Mo. *Phys. Rev. B* **1999**, *60*, 8383–8387.
25. Alam, Md. K.; Yaghoobi, P.; Nojeh, A. Unusual Secondary Electron Emission Behavior in Carbon Nanotube Forests. *Scanning* **2009**, *31*, 221–228.
26. Futaba, D. N.; Hata, K.; Namai, T.; Yamada, T.; Mizuno, K.; Hayamizu, Y.; Yumura, M.; Iijima, S. 84% Catalyst Activity of Water-Assisted Growth of Single Walled Carbon Nanotube Forest Characterization by a Statistical and Macroscopic Approach. *J. Phys. Chem. B* **2006**, *110*, 8035–8038.
27. Esconjauregui, S.; Xie, R.; Fouquet, M.; Cartwright, R.; Hardeman, D.; Yang, J.; Robertson, J. Measurement of Area Density of Vertically Aligned Carbon Nanotube Forests by the Weight-Gain Method. *J. Appl. Phys.* **2013**, *113*, 144309–144316.
28. Berglund, C. N.; Spicer, W. E. Photoemission Studies of Copper and Silver: Theory. *Phys. Rev.* **1964**, *136*, A1030–A1044.